Russian Physics Journal, Vol. 54, No. 2, July, 2011 (Russian Original No. 2, February, 2011)

CONDENSED-STATE PHYSICS

PECULIAR BEHAVIOR OF STRUCTURE REARRANGEMENT IN NANOFIBER OF INTERMETALLIC Ni_3Al, CONTAINING LONG-PERIOD PAIRED THERMAL ANTI-PHASE BOUNDARIES, UNDER HIGH-RATE TENSILE UNIAXIAL LOADING ALONG <001>

A. I. Potekaev,[1] M. D. Starostenkov,[2] N. V. Sinitsa,[2] A. V. Yashin,[2] E. G. Kharina,[2] and V. V. Kulagina[3]

UDC 669.018

Using molecular dynamics simulations, peculiarities of structure rearrangement in nanofiber of intermetallic Ni_3Al containing long-period, paired, thermal (nonconservative) anti-phase boundarties (APBs is investigated in the course of high-rate, tensile uniaxial loading along <001>. Four main deformation stages are determined (quasi-elastic, plastic, material flow and rupture), with each stage revealing particular features of structure transformations and energy transfer. The presence of periodic thermal planar defects in the long-period nanostructure (combined thermal anti-phase boundaries) significantly affects the onset of plastic deformation. A change in the type of thermal APBs in the long-period structure in turn affects the time to total rupture of nanofiber under plastic deformation condition. For the thermal AA 1/2<110>{001}APBs, the time to total nanofiber rupture is slightly decreased, while that for the thermal AB 1/2<110>{001} APBs is considerably increased.

Keywords: long-period structure, deformation, structure rearrangement, deformation stages, yield strength.

INTRODUCTION

Currently, the condensed matter physics focuses its attention on condensed systems with nanosized periodic structure inhomogeneities. These are primarily semiconductor materials showing good promise as the basis for applications in nanoelectronics, a principally new level of electronics. Other promising systems are metals and their alloys, which in a nanocrystalline state exhibit unique properties as structural and functional materials. Of special interest in terms of research are the ordered alloys with long-period structure [1–10], with APBs being periodic structure defects [1, 11–22].

The purpose of this work is to investigate peculiar behavior of structure-energy transformations that occur in metal nanofiber with long-period, paired, thermal (nonconservative) APBs in the course of high-rate tensile uniaxial loading.

1. COMPUTER EXPERIMENT MODEL AND PROCEDURE

We investigated the mechanisms of structure rearrangement in a metal nanofiber containing periodic planar defects in the course of high-rate deformation by tensile uniaxial loading. The object under study is a model of an Ni_3Al

[1]V. D. Kuznetsov Siberian Physical Technical Institute at Tomsk State University, Tomsk, Russia, [2]Altai State Technical University, Barnaul,Russia, [3]Siberian State Medical University, Tomsk, Russia, e-mail: kanc@spti.tsu.ru; genphys@mail.ru. Translated from Izvestiya Vysshikh Uchebnykh Zavedenii, Fizika, No. 2, pp. 48–55, February, 2011. Original article submitted July 22, 2010.

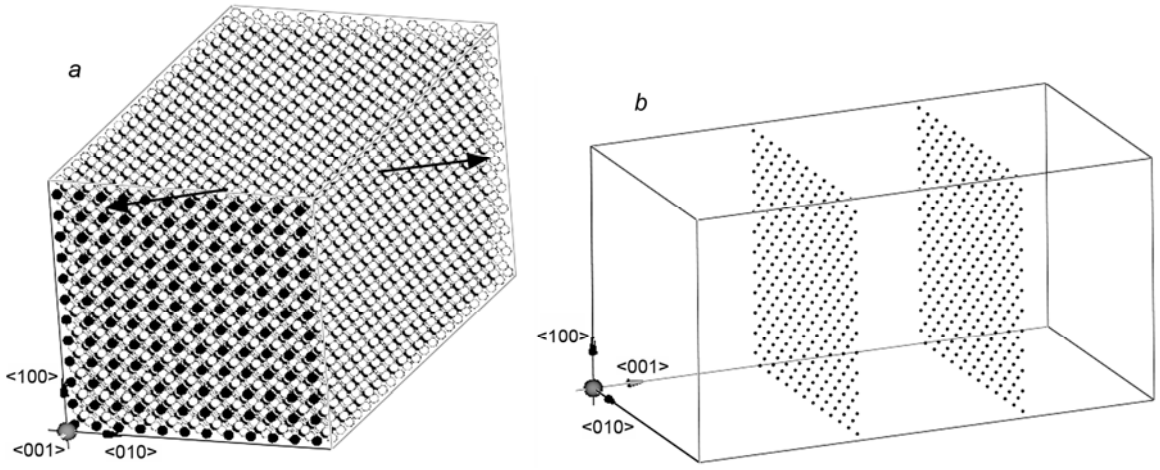

Fig. 1. Model of an Ni_3Al nanofiber: ideal nanofiber before introduction of APBs (*a*) and a scheme of introduction of two *AB* 1/2<110>{001}TAPBs (*b*).

intermetallic nanofiber (Fig. 1*a*), which contains paired equidistant thermal 1/2<110>{001} APBs (TAPBs) of the *AA* and *AB* types (distance between APBs is varied from 3 to 17 interlayers) (Fig. 1*b*). Let us introduce APBs one by one at equal distances from each other along the <001> direction so that their position would correspond to their geometrical equidistance from rigid boundaries (grips) and the nanofibers geometric center. This model corresponds to the $L1_2$(M) superstructure [1, 11, 12, 15, 22].

The experiment is to be carried out by the method of molecular dynamics using the Morse pair-potential functions [23–25], since the challenge consists in the principle physical mechanisms of structure transformations. Let us take the cutoff radius for pair interaction between the atoms to be 0.494 nm.

Write the potential energy of a system of N atoms as

$$E = \frac{1}{2} \sum_{i=1, i\neq j}^{N} \sum_{j=1}^{N} \varphi_{KL}\left(\left|\boldsymbol{r}_i - \boldsymbol{r}_j\right|\right), \tag{1}$$

where φ_{KL} is the atomic interaction potential of atoms of the K and L kinds, which are located in the sites with the radius-vectors $\boldsymbol{r}_i$ and $\boldsymbol{r}_j$, that is of the i-th and j-th atoms.

We carried out molecular dynamics simulations of nanofibers behavior [26–28]. To solve the system of ordinary differential equations, use was made of the numerical half-step Euler method.

In order to take into account the effects of energy-exchange of the model system with the surrounding medium, we applied an algorithm for velocity rescaling – the Berendsen thermostat [27].

The calculation grid of the nanofiber was constructed as a rectangular parallelepiped with a square base in plane (001) and height (nanofibers axis), which corresponded to <001>. The calculation grid measured 12×12×18 unit cells (4.07×4.07×6.20 nm^3). The total number of atoms was 10368. The boundary conditions used were mixed: free conditions along <100>, <010> and fixed conditions along <001>.

The dynamic uniaxial tensile deformation was simulated by a consecutive displacement of all atoms in the fixed boundaries along <001> by 0.002 nm every 0.1 ps, which corresponded to the strain rate $3.2 \cdot 10^9$ s^{-1}. The computer experiment temperatures were 10, 300 and 1100 K.

In order to analyze the defect structure evolution at the atomic level, we used a virtualized 3-D grid providing for possible rotation, scaling, and marking of atomic planes and displacements both with respect to the initial point of time and those between two selected time points.

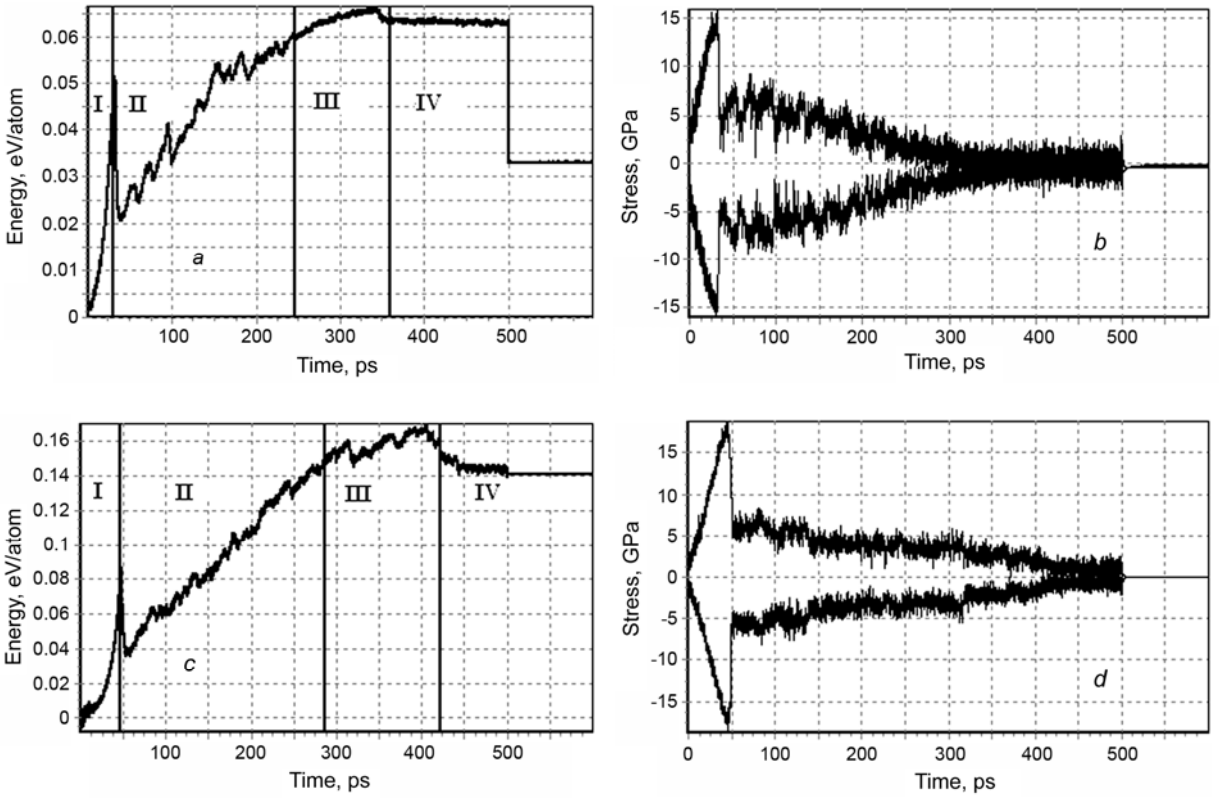

Fig. 2. Temporal dependences of deformation of nanofiber with paired *AA* 1/2<110>{001} TAPBs spaced by 9 layers, (*a*) and *AB* 1/2<110>{001} TAPBs (*c*), and the respective stresses on the grips (*b* and *d*) at 300 K.

2. RESULTS AND DISCUSSION

2.1. Effect of the antiphase period on mechanisms of deformation taking place in the long-period structure

In earlier works [29, 30] the authors revealed deformation stages of pure-metal, Ni and Al, and intermetallic, Ni_3Al, nanofiber with long-period shear-type APBs [22]. In this work we are going to look at the high-rate uniaxial tensile deformation of nanofiber from intermetallic Ni_3Al with different density of long-period, paired, thermal (nonconservative) APBs.

Structure deformation in the course of loading can be plotted as the time dependences of deformation energy and stress built-up on the grips (Fig. 2). The calculations at 10, 300 and 1100 K yielded similar results.

Let us consider the deformation stages observed during calculations.

Stage one – quasi-elastic deformation. The first stage of deformation is characterized by displacement of atoms with respect to their initial equilibrium. It should be noted that no irreversible structure deformation is observed, while stress on the grips is continuously increased. In the central part of the nanofiber its cross-section is seen to decrease (Fig. 3). When the type of introduced paired 1/2<110>{001} TAPBs is changed from *AA* to *AB* , the length of the first stage slightly varies within 1–5 ps. In particular, upon introduction of a paired *AA* 1/2<110>{001} TAPB quasi-elastic deformation lasts 30 ps, and for an *AB* 1/2<110>{001} TAPB – 34 ps.

An analysis of the temporal behavior of stress on the grips (Fig. 2*b* and *d*) at different temperatures showed that the end of the first stage is characterized by a significant drop of stress. The decrease in stress by the end of the first stage is observed for all types of nonconservative APBs. The value of stress on the grips is decreased with increase in

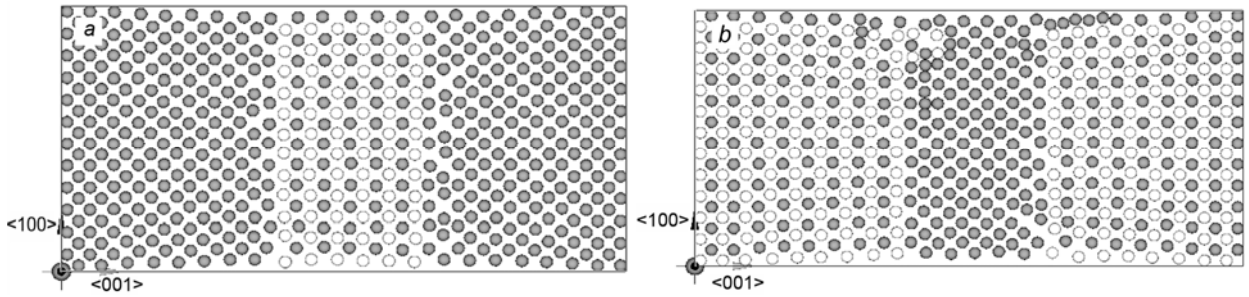

Fig. 3. Structural deformation of nanofiber with a paired *AB* 1/2<110>{001}TAPB at a distance of 9 layers in the first stage: 33-rd ps, plane {010} (*a*) and 35 –th ps, plane {010}(*b*).

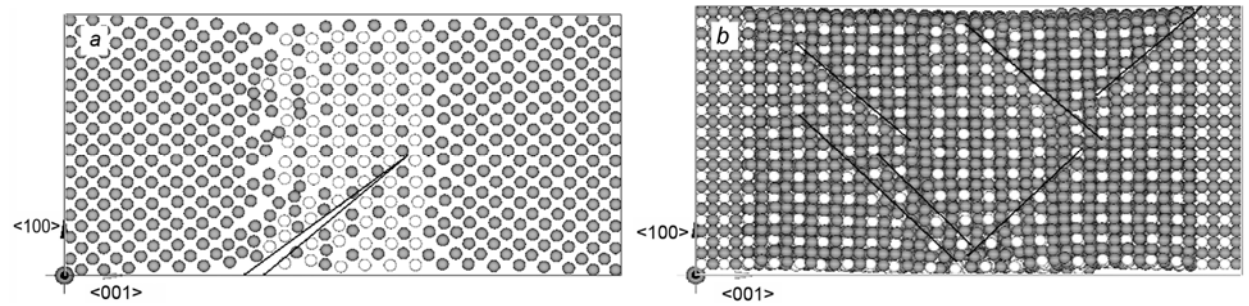

Fig. 4. Regions of deformation nucleation at the 31-st ps of the experiment at 300 K (*a*) and slip lines appearing in nanofiber at the 35-th ps at 300 K (*b*).

the temperature and so is the value of the deformation energy buildup. The decrease in stress coincides in time with the relief of the built-up deformation energy (Fig. 2).

The end of the stage of quasi-elastic deformation is characterized by relaxed regions of nucleation of plastic deformation (Fig. 4*a*) and formation of a shear-dislocation shelf (Fig. 4*b*). There is an intensive formation of anti-phase domains (APDs), which predominantly move along planes {111}. Given seven or more layers between the introduced paired APBs in the place of the APD sliding, and in the case of complete slip of APDs by one plane with respect to the axis of deformation, the fcc-structure is restored.

As the distance between the introduced APBs is increased, the deformation nucleation region is located in one of the 1/2<110>{001}TAPBs, this being an APB of the *AB*-type in 100 % of the experiments, contrary to the case with the APBs of the *AA*-type, where the percentage of nucleation is within 70–85%.

It should be noted that as the density of APBs is increased, the region of deformation nucleation would always be located at the junction of two paired defects – at the anti-phase boundary. Thus, the deformation region is localized in the vicinity of the APB closest to the site of deformation localization (Fig. 5).

Stage two – plastic deformation. It is well known that the driver of plastic deformation is the slip process. The onset of the second stage is characterized by sliding of the parts of nanofiber with respect to each other, slip lines appear on the surface, and shelves are formed, these are shear dislocations outcropped to the surface (Fig. 6*a*). It is clear from Fig. 6*b* that there is an intensive slipping predominantly along planes {111}, indicating a process of active structure rearrangement.

The structure-energy transformation in the stage of plastic deformation is clearly depicted by the time dependence (Fig. 7) of the number of atoms corresponding to the hcp (curve *1*) and intermediate (curve *2*) coordinations of the nearest neighbors. The presence of atoms with the respective hcp-neigborhood allows us to get an isight into the internal structure rearrangement of nanofiber.

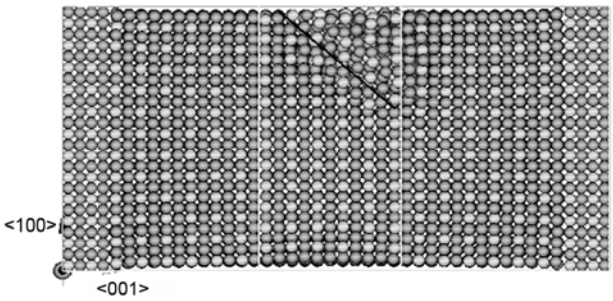

Fig. 5. Regions of deformation localization for a paired 1/2<110>{001} TAPB at a distance of 9 layers.

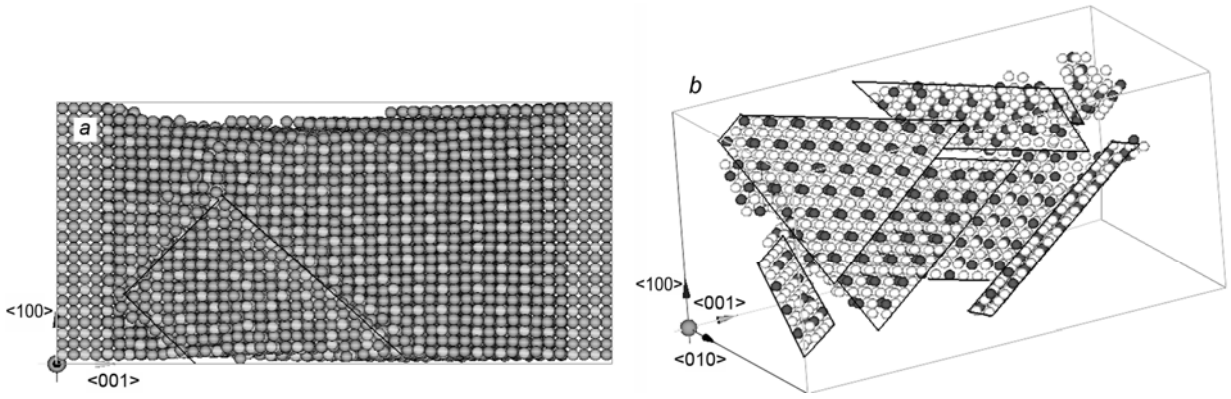

Fig. 6. Atomic structure rearrangement at the 50-th ps for a paired 1/2<110>{001} TAPB at the temperature 300 K at a distance of seven layers: plane {010} (*a*) and slip of the nanofiber parts along planes {111} (*b*).

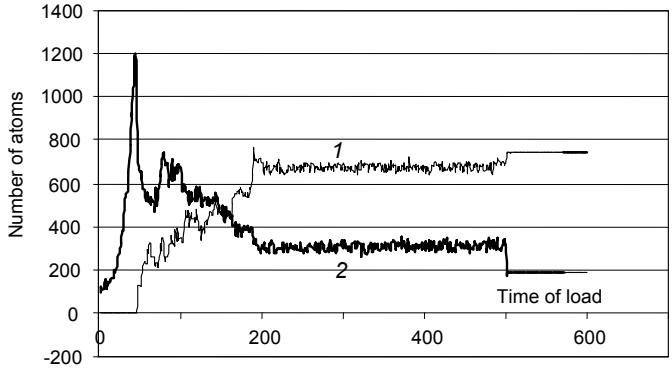

Fig. 7. Dependence of the number of fcc-atoms (curve *1*) and intermediate (curve *2*) nearest neighborhood on time in Ni_3Al nanofiber with seven layers between the *AA* 1/2<110>{001} TAPBs at the temperature 300 K.

The peak at the 32-nd ps (Fig. 7) corresponds to a planar slip along {111} followed by the formation of an amorphous slip region not on one {111} but on a number of planes. Two APDs are observed to form above and below the slip plane. The increase in the hcp-phase is evidence of the dynamic slip process. The large number of hcp-atoms at the 500-th ps implies an incomplete reconstruction of the hcp-structure with a large number of shelves –

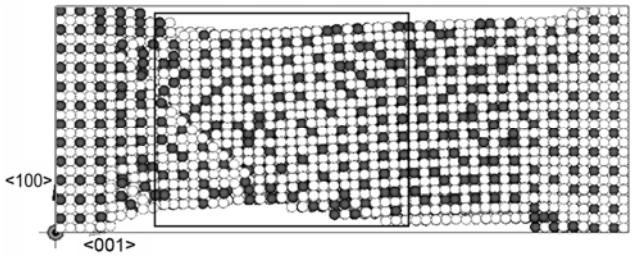

Fig. 8. Partial recovery of the hcp-structure at the 140-th ps with five atomic layers between the 1/2<110>{001} TAPBs at the temperature 300 K.

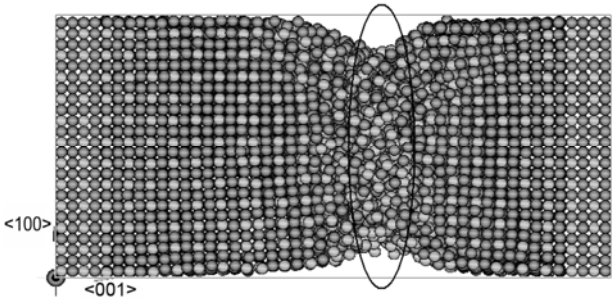

Fig. 9

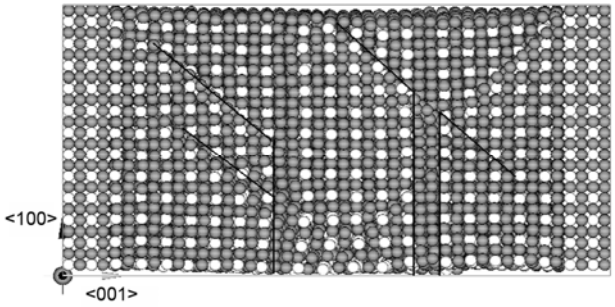

Fig. 10

Fig. 9. Localization of shear at the *AB* -type APB in the fcc-structure at the 125-th ps with seven layers between the TAPBs 1/2<110>{001} at the temperature 300 K.

Fig. 10. Slip of the fcc-structure at the 120-th ps with seven layers between TAPBs 1/2<110>{001} at the temperature 300 K.

dislocations outcropped to the surface (Fig. 8). For different types of TAPBs, *AA* and *AB*, there is a cyclic slip of parts of nanofiber and reconstruction of the hcp-structure.

The features of rearrangement accompanying plastic deformation are as follows. The zone of deformation is characterized by a predominant slip along planes {111}. If an APB of the *AB*-type is introduced, nucleation of deformation and further shears in the region of deformation are observed at one of the APBs (Fig. 9). In the case of a second long-period APB on the path of the shear, the slip is localized at this boundary. The APD is displaced with respect to plane {111} followed by the recovery of the fcc-structure in the slip region (Fig. 10).

If the region of deformation is located between two long-period APBs, then slip of the part of nanofiber occurs only within these defects (Fig. 9) followed by recovery of the fcc-structure. This peculiar feature is observed for all the series of computer experiments run with different number of long-period APBs.

In other words, during nanofiber slip the deformation is localized on the nearest APBs and does not go beyond. In this stage, a cyclic process is realized, which includes 'slip of nanofiber parts – shear localization on long-period APBs – recovery of fcc-structure'. It should be noted that when the number of layers between APBs is less than seven, no effect of the boundary period on the slip during nanofiber structure rearrangement in the stage of plastic deformation is observed, which could be accounted for by the low energy of this planar defect.

Stage three – flow. In the third stage of deformation (flow) the structure rearrangements occur in the region of the neck only, without any changes in the bulk. The deformation energy built up in the course of material flow varies by no more than 0.01 eV/atom. At the 350-th ps the nanofiber fails (Fig. 11). The effect of the antiphase period on structure rearrangements is not observed.

TABLE 1. Time Intervals of the Deformation Stages

Time	Layer type	3 layers	5 layers	7 layers	9 layers	11 layers	13 layers	15 layers	17 layers
Onset of plastic deformation	**AA**	31	31	31	31	30	30	30	30
	AB	35	34	35	32	33	34	34	34
Nanofiber rupture	*AA*	340	385	390	370	325	330	350	325
	AB	470	480	470	460	490	560	560	550

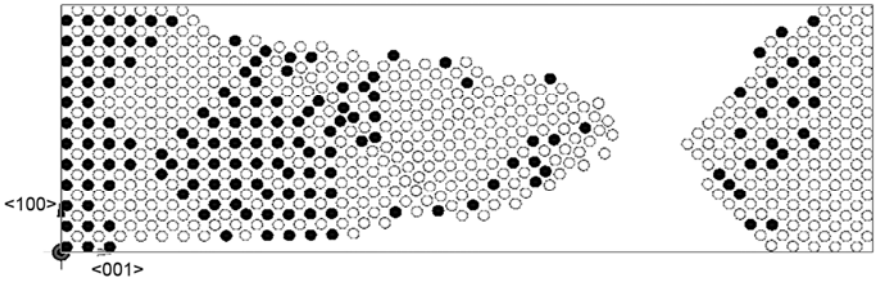

Fig. 11. Rupture of nanofiber at the 350-th ps for seven atomic layers between paired TAPBs *AA* 1/2<110>{001} at the temperature 300 K.

Stage four – failure. After failure and relaxation by superfast cooling to 0 K, there are APDs in nanofiber, which were formed earlier in the stage of plastic deformation. After relaxation, the fraction of atoms with the hcp-neigborhood is below 2.5% of the total number. The total number of atoms having the hcp-neigborhood is 95%, which indicates a nearly complete recovery of the fcc-structure and disappearance of the stalking faults.

It should be noted that peculiarities of deformation behavior of metallic nanofiber of Ni_3Al containing long-period paired thermal (nonconservative) APBs are very close to the behavior of this nanofiber with long-period shear-type (non-conservative) APBs [22].

2.2. The effect of the antiphase period on temporal intervals of the onset of plastic deformation and the time to complete failure of the nanofiber with a long-period structure

In order to study the effect of periodic thermal APBs on the temporal features of deformation in the nanostructure, we calculated the time intervals of the onset of the stage of plastic deformation and the time to complete nanofiber failure for different APB densities (Table 1).

An analysis of the data obtained demonstrated that the time of onset of plastic deformation is 31–34 ps, with the maximum variation of as low as 2–4 ps, i.e., less than 0.5% of the maximum deformation time. The pattern of structure-energy transformations by the 31–34 ps of the quasi-elastic stage is as follows. In the course of quasi-elastic deformation the atoms are symmetrically displaced from their initial positions under loading. By the onset of plastic deformation a number of point defects are observed to form (vacancies, interstitial atoms and substitution point defects). Stress on the grips increases in a linear fashion, and by the 30–33-rd ps the maximum deforming stress is built in the nanofiber. Parts of the nanofiber undergo slip to form new defects.

A comparison of the time of onset of plastic deformation with the data from [29] reveals that in a perfect nanofiber the time of the onset of the second stage of deformation is longer (52–55 ps). The rupture time of a nanofiber containing thermal (nonconservative) APBs exceeds that in the fiber with shear (conservative) APBs [22].

Thus, the presence of periodic planar defects such as thermal APBs of the *AA* and *AB* type in the long-period structure only insignificantly affects the time of the onset of plastic deformation. As the number of atomic layers between the paired *AA* 1/2<110>{001} TAPBs is increased, the time of quasi-elastic deformation is slightly decreased.

On the other hand, when we introduce combined APBs, a change in the number of layers between thermal APBs in the nanofiber results in a longer delay in the time of the onset of plastic deformation.

Another important characteristic of the deformation process is the time of nanofiber rupture. Table 1 presents the values of time to complete rupture in nanofibers with different density of APBs. It is clearly seen that as the number of layers between the *AA* 1/2<110>{001} TAPBs is increased, the time to complete rupture is slightly decreased. In particular, for three layers between the introduced APBs the time to complete rupture is 340 ps, while for 17 layers it is 325 ps. As the type of the introduced APB is changed from *AA* to *AB*, the time to complete rupture is also increased. For instance, for 3 layers it is 470 ps, and for 17 layers it is already 550 ps.

Thus, a change in the type of the thermal paired APBs in the long-period structure considerably affects the variation of the time intervals to complete rupture of the nanofiber under plastic deformation. In the case of an *AA* 1/2<110>{001} TAPB, when the number of layers between the APBs is increased, the time to complete rupture is insignificantly decreased, and in the case of an *AB* 1/2<110>{001} TAPB it is considerably increased.

SUMMARY

Based on the analysis of the structure-energy transformations taking place in the long-period structure of nanofiber of intermetallic Ni_3Al with periodic paired thermal (nonconservative) APBs in the course of high-rate uniaxial tensile loading, four main deformation stages have been revealed: quasi-elastic, plastic, flow, and rupture. It has been found out that the structure-energy transformations in the intermetallic Ni_3Al nanofiber with periodic thermal (nonconservative) APBs in the course of high-rate uniaxial tensile loading are very close to those in the same nanofiber with long-period shear-type APBs [22].

The presence of periodic planar defects like thermal *AA* and *AB* APBs in the long-period structure insignificantly affects variation in the time of onset of plastic deformation. As the number of atomic layers between the embedded paired *AA* 1/2<110>{001}TAPBs is increased, the time interval of the stage of quasi-elastic deformation is slightly decreased. However, in the case of a combined-type TAPB the changing number of atomic layers noticeably affects the onset of plastic deformation.

A change in the type of thermal paired APBs in the long-period structure exerts a strong influence on variation in the time to complete rupture of nanofiber under plastic deformation conditions. In the case of an *AA* 1/2<110>{001}TAPB embedded into the material, the time to complete rupture is slightly decreased as the number of atomic layers is increased, while for an *AB* 1/2<110>{001}TAPB it is considerably increased.

REFERENCES

1. A. I. Potekaev, I. I. Naumov, V. V. Kulagina, *et al*., Natural Long-Period Nanostructures [in Russian] (Ed. A.I. Potekaev), Tomsk, NTL Publ. (2002).
2. A. I. Potekaev, A. A. Klopotov, E. V. Kozlov, and V. V. Kulagina, Low-Stability, Pretransitional Structures in Titanium Nickelide [in Russian] (Ed. A. I. Potekaev), Tomsk, NTL Publ. (2004).
3. A. I. Potekaev, M. D. Starostenkov, A. M. Gleizer, *et al*., Structure-Phase States and Properties of Metallic Systems [in Russian], (Ed. A. I. Potekaev), Tomsk, NTL publ. (2004).
4. V. E. Gromov, A. I. Potekaev, and M. D. Starostenkov, Structure-Phase States of Promising Materials [in Russian], Novokuznetsk, NPK Publ. (2009).
5. V. N. Udododv, A. I. Potekaev, V. V. Kulagina, *et al*., Simulation of Phase Transformations in Low-dimensional Defect Nanostructures [in Russian], Abakan, Khakassiya Uni. Publ. (2008).
6. S. V. Dmitriev, N. N. Medvedev, A. I. Potekaev, *et al*., Russ. Phys. J., No. 8, 858–865 (2008).
7. A. I. Potekaev, and V. V. Kulagina, Russ. Phys. J., No. 11/3, 148–150 (2008).
8. S. V. Dmitriev, A. I. Potekaev, A. A. Nazarov, *et al*., Russ. Phys. J., No. 2, 132–137 (2009).
9. A. I. Potekaev, E. A. Dudnik, M. D. Starostyenkov, and L. A. Popova, Russ. Phys. J., No. 10, 1053–1063 (2008).

10. S. V. Dmitriev, A. I. Potekaev, and A. V. Samsonov, Russ. Phys. J., No. 6, 622–639 (2009).
11. A. I. Potekaev, Russ. Phys. J., No. 6, 549–562 (1995).
12. A. I. Potekaev, Russ. Phys. J., No. 6, 521–533 (1996).
13. I. I. Naumov, A. I. Olemskoy, and A.I. Potekaev, Fiz. Met. Metalloved., **75**, Issue 6, 47–57 (1993).
14. A. I. Potekaev, Phys. Stat. Sol. (a), **134**, 317–334 (1992).
15. O. I. Velikokhatnyi, S. V. Eremeev, A. I. Potekaev, and I. I. Naumov, Pis'ma JETF, **69**, Issue 8, 548–554 (1999).
16. O. I. Velikokhatnyi, S. V. Eremeev, A. I. Potekaev, and I. I. Naumov, J. Experim. Theor. Phys. , 98, No. 3, 565–574 (2004).
17. O. I. Velikokhatnyi, S. V. Eremeev, A. I. Potekaev, and I. I. Naumov, J. Phys.: Conden. Matter., No. 14, 8763–8769 (2002).
18. O. I. Velikokhatnyi, S. V. Eremeev, A. I. Potekaev, and I. I. Naumov, Comput. Mater. Sci., **19**, Nos. 1–4, 275–284 (2000).
19. O. I. Velikokhatnyi, S. V. Eremeev, A. I. Potekaev, and I. I. Naumov, Phys.: Condens Matter. **12**, No. 41, 8825–8830 (2000).
20. O. I. Velikokhatnyi, S. V. Eremeev, A. I. Potekaev, and I. I. Naumov, JETF, 117, Issue 3, 548–558 (2000).
21. O. I. Velikokhatnyi, S. V. Eremeev, A. I. Potekaev, and I. I. Naumov, J. Experim. Theor. Phys., **90**, No. 3, 479–487 (2000).
22. A. I. Potekaev, M. D. Starosrenkov, N. V. Sinitsa, *et al*., Russ. Phys. J., No. 8, 818–826 (2010).
23. A. I. Tsaregorodtsev, N. V. Gorlov, B. F. Demianov, and M. D. Starostenkov, Fiz. Met. Metalloved., **58**, No. 2, 336 (1984).
24. S. V. Eremeev and A. I. Potekaev, Russ. Phys. J., No. 6, 646–656 (2005).
25. E. V. Kozlov, L. E. Popov, and M. D. Starostenkov, Izv. Vyssh. Uchebn. Zaved. Fiz., No. 3, 107–108 (1972).
26. V. V. Kulagina, S. V. Eremeev, and A. I. Potekaev, Russ. Phys. J., No. 2, 122–130 (2005).
27. M. D. Starostenkov, A. V. Markidonov, T. A. Tikhonov, and A. I. Potekaev, Izv. Vyssh. Uchebn. Zaved. Fiz., No. 9/2, 139–144 (2009).
28. H. J. C. Berendsen *et al*., J. Chem. Phys., **81**, No. 8, 3684–3690 (1984).
29. M. D. Starostenkov, A. V. Yashin, E. A. Dudnik, *et al*., Zh. Perspektivn. Mater., No. 7, 383–388 (2009).
30. M. D. Starostenkov, A. V. Yashin, N. V. Sinitsa, and E. A. Dudnik, CD disk, Proceedings of 12th International Conference on Fracture, Ottawa, Ontario, Canada, fin00236, 1–9 (2009).
31. J. Friedel, Dislocations, Pergamon press, Oxford (1964).